DIAGNOSTYKA, 2025, Vol. 26, No. 3

e-ISSN 2449-5220
DOI: 10.29354/diag/208618

APPLICATION OF ELECTROMAGNETIC INTERFERENCE-BP TECHNOLOGY IN MECHANICAL NOISE CONTROL OF SMALL DC ELECTRODES

Hui CAO [1, *], Xiaoyan ZHANG [2]

[1] Department of Basic Teaching, Henan Polytechnic Institute, Nanyang 473000, China
[2] Xinjiang Production and Construction Corps 13th Division Senior Vocational High School, Hami City 439000, China
[*] Corresponding author, e-mail: caohui1003@126.com

Abstract

With the widespread use of miniaturized electronic equipment in daily life, the problem of electromagnetic interference has become increasingly prominent, especially in precision instruments and communication equipment. To effectively reduce the causes of mechanical noise generated by small DC electrodes during operation and the electromagnetic interference effects on surrounding equipment, a mechanical noise control method that combines piezoelectric impedance technology and back-propagation neural networks is proposed. In the process, small DC motor electrodes were used as the research object, and the sources of mechanical noise generated by the motor were analyzed. At the same time, different analysis software was used to simulate and model the stator and rotor of the motor. The results show that when different algorithms are run on the training set and test set, when the amount of data increases to 560 and 1120 respectively, the method constructed in the experiment has the maximum fitness value, with values as high as 98.98% and 97.86%. When the training set is run, when the running time increases to 0.894s, the accuracy of the method constructed in the experiment to control mechanical noise reaches 91.68%. The application effect shows that when the material of the stator shell is steel, the occurrence of the maximum natural frequency of the stator is affected by the elastic modulus, which is far greater than the influence of the material density. The experiment provides new ideas and methods for noise and electromagnetic interference control of small DC electrodes.

Keywords: mechanical noise; noise control; small DC electrode; electromagnetic interference; backpropagation neural network

1. INTRODUCTION

As the quick advancement of technology, small DC motors have become an indispensable part of modern industrial and consumer electronics. Their applications range from household appliances to precision medical equipment to complex industrial systems [1, 2]. However, as the complexity and performance requirements of these applications increase, the problem of mechanical noise generated during operation of small DC motors and electrodes has become increasingly prominent. These problems not only affect the performance and user experience of the device, but may also pose a threat to the stability and reliability of the electronic device [3, 4]. Among traditional solutions, mechanical and electrical improvements are common approaches, but these techniques often need to be performed during the design phase and can add cost and complexity. In recent years, with the rise of artificial intelligence and machine learning technology, new solutions have been provided for the control of mechanical noise [5]. In particular, the back propagation (BP) algorithm shows great potential in optimization problems, which provides new possibilities for noise control of small DC motors and electrodes. In view of this, the experiment aims to explore an innovative method to control and analyze the source of mechanical noise of small DC motors by combining electromagnetic interference (EMI) analysis and BP technology. First, the experiment analyzes in detail the mechanism of noise and electromagnetic interference generated by small DC motors during operation, and identifies key factors and influencing paths. Then, these factors will be modeled and simulated using the BP algorithm to optimize the motor design and analyze the sources of noise.

A control method of mechanical noise of small DC electrode combined with EMI analysis and BPNN is proposed, which effectively reduces the mechanical noise and improves the operation efficiency and reliability of the equipment. This method not only optimizes the equipment performance and reduces energy consumption, but also significantly reduces

Received 2024-07-10; Accepted 2025-07-24; Available online 2025-08-01

noise pollution and improves the working environment and quality of life. In addition, by reducing electromagnetic interference, the stability and reliability of electronic equipment are improved. The proposed method provides important technical reference for industrial and consumer electronics fields, promotes the development and application of related technologies, and is of great significance to environmental protection and sustainable development.

The manuscript is composed of four parts. The first part is a summary of related domestic and foreign technologies; the second part is the construction of the experimental method; the third part is the modeling, simulation and performance analysis of the experimental method; the fourth part is the summary of the results of the entire article. Summarize and look forward to future research. Fig. 1 shows the research flow framework.

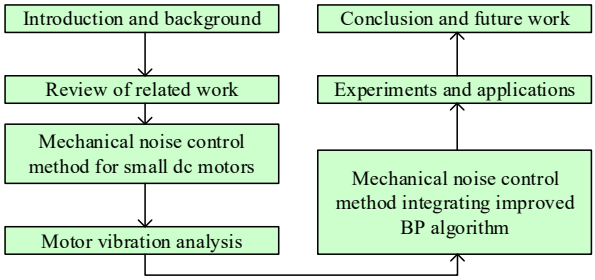

Fig. 1. Research flow

2. RELATED WORKS

In the field of modern electronic engineering, small DC electrodes have attracted much attention because of their wide application in various electronic devices. While these electrodes provide the necessary power transmission and conversion functions, they also present a series of technical challenges. For this reason, many scholars have analyzed the detection methods of mechanical noise generated during the operation of DC motors and electrodes. Xu C et al. proposed an electrochemical seismometer for seabed exploration based on a new sensor electrode structure. The process of the sensing electrode is effectively simplified, and an insulating ring is used to adjust the space between the two electrodes. The seismometer was applied to natural earthquake detection and it was found that the correlation coefficient between the seismometer and the local seismic station was as high as 0.95; and it could operate well on the seabed [6]. In order to find the best energy storage system in electric vehicles, scholars such as Abd Aziz MA introduced a battery energy storage system (BESS) into the operation of the vehicle. The results showed that BESS were a reliable source and that stand-alone supercapacitors had the shortest runtime. At the same time, the energy management control strategy can be adjusted to effectively reduce the energy discharge rate of the capacitor [7]. In order to alleviate the impact of high temperature generated by DC arc on the safety of equipment and operators, Abdullah et al. raised an adaptive detection method based on improved series DC arc fault. This method enables the detection of arc events using the current generated by the system. Thousands of tests under various conditions found that this method is highly effective and can be verified by arc detectors [8]. Jiang and other scholars proposed a new type of flexible and stretchable multi-biopotential sensing dry active electrode, which is composed of electrodes, soft substrates and simple circuits. The circuit substrate is molded from silicone resin and implemented on a patterned substrate. Experimental tests found that the sensor and system can produce good signal quality for a variety of biological potentials [9]. Krasecki et al. raised a design method based on a hybrid classical quantum computer. In the process, chemical media, electrode interfaces, etc. are combined with the computer to obtain a classical feedback loop. The results show that in the presence of experimental noise, the local minimum value obviously converges to the global minimum value, which has obvious scalability [10].

Meanwhile, massive scholars have analyzed the control methods of mechanical noise. To control the output flow of a counter-rotating cylinder, Xu et al. proposed a deep reinforcement learning-based artificial neural network control method. During the process, two smaller rotating cylinders were used for experiments, and the results showed that the interaction between the rotating small cylinder and the main cylinder wake can effectively stabilize the periodic shedding phenomenon of the main cylinder microwave [11]. In order to effectively regulate the fuel usage of aircraft engines, Cao's team proposed an electronic engine fuel control system. During the process, experiments related to electromagnetic pulses were established, and wavelet transform was applied to perform time-frequency processing on the generation of induced voltage signals. In addition, an electromagnetic interference suppression method based on time domain and frequency domain is proposed to achieve effective control of electromagnetic pulse coupling interference [12]. To analyze the effect of feedforward neural network operation on signal propagation, scholars such as Ge and Wang proposed a fusion method based on Gaussian colored noise and electromagnetic radiation. Compared with the absence of electromagnetic radiation, the presence of electromagnetic radiation can slightly reduce the propagation of weak signals, and the feedforward nerves considered in the experiment can observe more complex structures [13]. In order to adjust the hydraulic power and control parameters of the unmanned walking platform, Wang and other scholars proposed a control strategy based on dual-relative control parameters in dual-loop PID. During the experiment, a model speed response model was established, and a simplified neural structure PID was introduced to form a hybrid neural network to control the engine speed and variable pump pressure. The outcomes denote that the control effect of this algorithm is very stable and can effectively adjust and control parameters [14]. To control the heating process

of the heating furnace, Wang and other scholars proposed a PID control optimization algorithm based on genetic algorithm and the economic Backpropagation neural network (BPNN). During the process, MATLAB software was used to conduct experiments on the heating furnace of the research object. The data showed that the dynamic characteristics of the system were excellent and the robustness was strong [15].

In summary, although massive scholars in this field have conducted research on neural network algorithms and DC motor fault detection, they have revealed the knowledge structure and development trends in this field, and also identified key issues and problems in the research. Potential research gaps. However, there are still some issues and research space that have not been fully explored. For example, there is still little research in the field of motor stators, and electromagnetic interference and artificial intelligence methods have not yet been widely used in practice. In view of this, the experiment proposes a DC motor mechanical noise control method based on electromagnetic interference and BPNN, and looks forward to obtaining new research methods.

3. SMALL DC MOTOR MECHANICAL NOISE CONTROL METHOD INTEGRATING EMI-BP

In modern motor applications, especially in the field of small DC motors, mechanical noise issues have always been a key challenge affecting performance and reliability. To effectively address this issue, the research proposes an innovative control method, which is a small DC motor mechanical noise control method that combines EMI theory and back-propagation neural network algorithm.

3.1. Motor vibration analysis based on piezoelectric impedance technology

With the advancement of mechanical and electrical equipment, motors have become more and more popular, but at the same time, they have also attracted the attention of all walks of life and many scholars on motor vibration and noise [16]. The experiment mainly focused on the problem of mechanical noise in small DC motors. Under heavy load, the balls of the motor bearing will produce elastic deformation when they contact the outer ring raceway. The deformation of this raceway will change periodically with the movement of the contact point, resulting in vibration and mechanical noise. These vibrations and mechanical noise are usually caused by the electromagnetic force inside the motor [17]. When building a motor vibration analysis model, the motor is usually regarded as a mechanical system containing multiple parameters (such as degrees of freedom, mass, stiffness). Since the mass stiffness and degrees of freedom of the vibration system are different, the electromagnetic force of the electrodes in the motor and the different components have different impacts on the vibration of the system. By analyzing the vibration equation, the mathematical vibration model of the system is established see Equation (1).

$$[M]\{\ddot{x}\}+[C]\{\dot{x}\}+[K]\{x\}=\{F(x)\} \tag{1}$$

Equation (1), $[M]$ means the mass matrix of the system; $[C]$means the damping matrix of the system; $[K]$means the stiffness matrix of the system; $\{x\}$means the displacement vector; $\{\dot{x}\}$means the velocity vector, i.e., the first derivative of displacement with respect to time; $\{\ddot{x}\}$means the acceleration vector, i.e., the second derivative of displacement; $\{F(x)\}$ denotes vibration excitation. The calculation of the approximate value of the damping matrix of the system is shown in Equation (2).

$$[C]=a[M]+b[K] \tag{2}$$

After determining the damping matrix of the system, the differential equations can be calculated through the characteristic equation, and the relative value of the amplitude can be calculated, see Equation (3).

$$[P]=\left[\{A^{(1)}\}\{A^{(2)}\}\cdots\{A^{(3)}\}\right]=\begin{bmatrix}A_1^{(1)} & A_1^{(2)} & \cdots & A_1^{(n)}\\ A_2^{(1)} & A_2^{(2)} & \cdots & A_2^{(n)}\\ \vdots & \vdots & & \vdots\\ A_n^{(1)} & A_n^{(2)} & \cdots & A_n^{(n)}\end{bmatrix} \tag{3}$$

Equation (3), $[P]$ represents the amplitude. Then, $[P]$ the vibration excitation source obtained after regularization and decoupling is shown in Equation (4).

$$F(t)=F_0e^{j\omega t} \tag{4}$$

Equation (4), $F(t)$ represents the vibration excitation source. Solving the equations can obtain the solutions to the non-homogeneous differential equations and vibration equations, see Equation (5).

$$x=e^{-\delta t}(Ae^{j\omega_0 t}+Be^{-j\omega_0 t})+\varepsilon e^{j\omega t} \tag{5}$$

In Equation (5), $e^{-\delta t}(Ae^{j\omega_0 t}+Be^{-j\omega_0 t})$ represents the transient response; $\varepsilon e^{j\omega t}$represents the steady-state response. Since it is very complex to calculate the damping of small DC motors and electrodes, the experiment is combined with complex modal theory to calculate the vibration equation with multiple degrees of freedom. The corresponding calculation is denoted in Equation (6).

$$\begin{cases}x_i(t)=\sum_{i=1}^{n}\eta_{ir}P_{\mathrm{r}}\left[e^{j(\beta_r+\gamma_{ir}+\theta_i)}+e^{-j(\beta_r+\gamma_{ir}+\theta_i)}\right]=2\sum_{i=1}^{n}\eta_{ir}P_{\mathrm{r}}e^{-\alpha_r t}\cos(\beta_r t+\gamma_{ir}+\theta_r)\\ [M]\{\ddot{x}\}-[M]\{\dot{x}\}=0\end{cases} \tag{6}$$

Equation (6), $[M]\{\ddot{x}\}-[M]\{\dot{x}\}$ represents the auxiliary equation; $i$represents the pointing; represents η_{ir} the level modal coefficient γ_{ir} of r the pointing ; represents the modal $i$phase angle of P_r the $r$pointing

order; i and θ_r represents the modal coordinate amplitude and modal coordinate phase angle; α_r and β_r represents the complex mode Real and imaginary parts of frequency. In the operation of small DC motors, a piezoelectric effect occurs between the positive and negative electrodes. This effect causes charge transfer within the electrode. Even if the electric field disappears, a part of the polarization charge will still remain inside the piezoelectric material, thereby exhibiting a certain piezoelectric effect. Piezoelectric materials have a unique property that they can generate electrical signals when acted upon by external forces. This is due to the relative displacement of internal charges, which converts mechanical energy into electrical energy. This process is called the positive piezoelectric effect. In contrast, the inverse piezoelectric effect involves the mechanical deformation that occurs when a voltage is applied to a piezoelectric material, achieving the conversion of electrical energy into mechanical energy. Since piezoelectric ceramic materials have both forward and reverse piezoelectric effects, they can be broadly utilized in research fields such as health detection and damage identification of electrode sensors and driving materials [18]. Piezoelectric impedance technology (Electromagnetic Interference, EMI) mainly uses the coupling effect between the piezoelectric ceramic material and the object to be measured to detect the inherent characteristics of the object to be measured. The experimental flow of EMI technology is shown in Fig. 2.

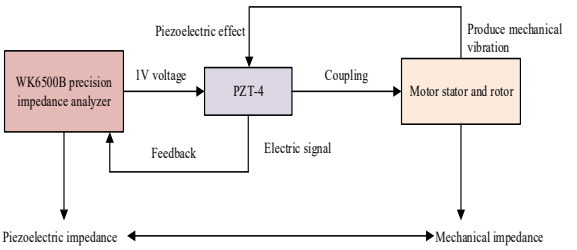

Fig. 2. Experimental process of piezoelectric impedance

The coupling system formed between the piezoelectric material and the measured object can be regarded as a comprehensive system with spring, mass and damping, referred to as SMD (Spring-Mass-Damper) system. The architecture of the SMD system constructed in the experiment is denoted in Fig. 3.

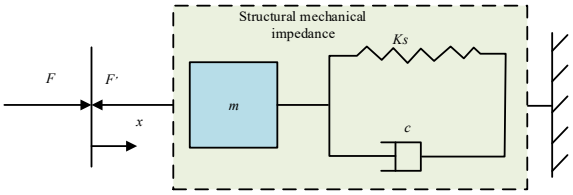

Fig. 3. Architecture of SMD system

The relationship between the excitation force and the resulting displacement can be obtained through the mechanical impedance of the system. Among many piezoelectric materials, piezoelectric ceramics (PZT)-4 material has both good receiving performance and emitting capability, while other types of PZT materials usually only have a single function. Therefore, PZT-4 was selected in the experiment to analyze the electrical impedance characteristics between the structure and piezoelectric coupling. The coupling effect of the obtained SMD system and PZT-4 is shown in Fig. 4.

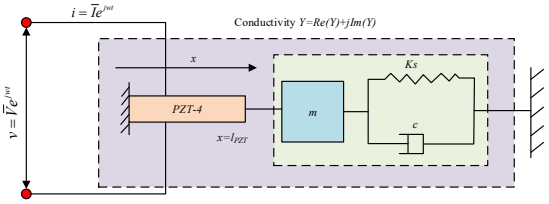

Fig. 4. Coupling effect between SMD system and PZT-4

Fig. 4, the DC motor is mainly composed of a stator and a rotor, and there is an obvious air gap between them. The distinguishing feature of an electric motor is its armature which has a commutating function. The stator part includes the housing, permanent magnets and bearings, where the permanent magnets are the main components that generate the air gap magnetic field. The rotor consists of a rotor core, windings, commutator and shaft. The rotor core is made up of multiple silicon steel sheets, with even tooth slots distributed on them for placing windings. As a mechanical rectifier component, the commutator is responsible for changing the direction of current. Each commutator segment on it is insulated from each other. The specific structure and 2D diagram of the motor are shown in Fig. 5.

3.2. Control method of mechanical noise of small DC motors integrating improved bp

The vibration noise of small DC motors belongs to the category of sounds that can be heard by humans, and involves the acoustic characteristics, structural vibration and modal analysis of the motor. Among them, the structural parameters of the motor stator have a critical impact on the modal frequency of the motor. One of the main reasons why the motor vibrates is that the modal frequencies of the stator and rotor are similar, resulting in resonance between them. To avoid this resonance phenomenon, it is necessary to adjust the modal frequencies of the two and ensure that their resonance frequency bands do not overlap. In recent years, artificial intelligence algorithms have begun to emerge, creating new opportunities for analyzing modal simulation and modal frequency of small DC electrodes. Artificial Neural Network (ANN) is a mathematical model based on mathematical statistical learning methods and optimization algorithms, which can analyze the modal frequencies between the stator and the rotor [19-21]. ANN can be divided into three categories: feedforward neural network, recurrent neural network and conventional feedback neural network [22, 23]. BPNN is a kind of ANN algorithm. For BPNN, the improvement of its performance and accuracy relies on continuous training of large amounts of data. During training, the network gradually learns and adjusts its internal parameters to better adapt and

predict new data sets [24, 25]. Through the BPNN, the obtained DC motor training sample data is first input into the BPNN, which is generally divided into 30% training set and 70% test set. Then the network structure is initialized with weight operations, and the training error function, calculation accuracy, learning rate and maximum number of learning times of the network are set and calculated. Among them, the kth sample is randomly selected from the sample data set. The calculation of the actual output and expected output of this sample is shown in Equation (7).

$$\begin{cases} x(k) = (x_1(k), x_2(k), \cdots, x_n(k)) \\ d(k) = (d_1(k), d_2(k), \cdots, d_n(k)) \end{cases} \quad (7)$$

In Equation (7), $d(k)$ represents the actual output; $x(k)$ represents the expected output. Then, the specific values of the input and output of different neurons in the hidden layer can be obtained by using the input of the actual sample, the connection weight and the interference factor, see Equation (8) [26, 27].

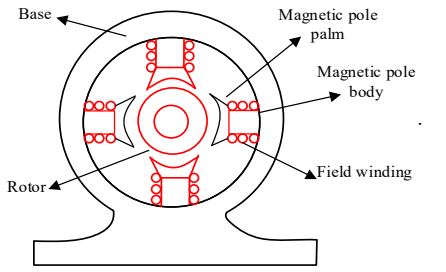

(a) Section view of a small DC motor

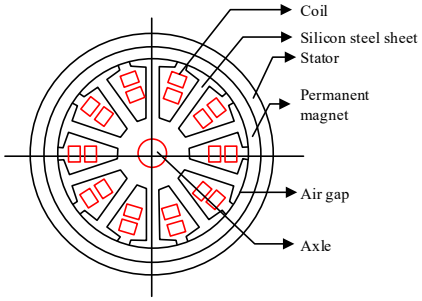

(b) 2D diagram of a small DC motor

Fig. 5. Specific Composition and Structure of Small DC Motor

$$\begin{cases} hid_{in}(k) = \sum_{i=1}^{n} w_{ij} x_i(k) - b_n \\ hid_{out}(k) = f(hid_{in}(k)) \\ yi_o(k) = \sum_{i=1}^{p} w_{ij} hid_{out}(k) - b_l \\ yo_l(k) = f(yi_o(k)) \end{cases} \quad (8)$$

In Equation (8), w represents the weight of the connection; b represents the interference factor; $hid_{in}(k)$ represents the input value of the corresponding neuron; $hid_{out}(k)$ represents the output value of the corresponding neuron. The partial derivatives corresponding to different neurons are calculated by combining the actual output and the expected output, see Equation (9).

$$-\delta_o(k) = \frac{\partial e}{\partial yi_o} = \frac{\partial\left[\left(\frac{1}{2}\sum_h^q (d_o(k) - yo_o(k))\right)^2\right]}{\partial yi_o} \quad (9)$$

In Equation (9), $\delta_o(k)$ represents the partial derivative. Then the new partial derivative is obtained through simplification, see Equation (10).

$$\frac{\partial e}{\partial hi_h(k)} = -\delta_h(k) \quad (10)$$

Then the calculation obtained by correcting the weight $wh_o(k)$ by the partial derivative $\delta_o(k)$ is shown in Equation (11).

$$\begin{cases} \triangle wh_o(k) = -\mu \frac{\partial e}{\partial wh_o} = \mu \delta_o(k) ho_h(k) \\ w_{h_o}^{N+1} = w_{h_o}^{N} + \mu \delta_o(k) ho_h(k) \end{cases} \quad (11)$$

In Equation (11), $ho_h(k)$ represents the attenuation function, which gradually decreases with the increase of iteration times. Finally, the calculation of the global error value of the network can be obtained as shown in Equation (12).

$$E = \frac{1}{2m}\sum_{k=1}^{m}\sum_{o=1}^{q}(d_o(k) - y_o(k))^2 \quad (12)$$

In Equation (12), Erepresents the global error. In the application process of BPNN, the termination condition of network training is usually set as the error threshold or the number of iterations. Training stops when the network's error drops below a preset threshold, or reaches a specific number of iterations. If the performance of the network does not meet the expected target, the network can be further trained by introducing new sample data. Applying BPNN to the prediction of motor structural parameters first requires establishing the network structure, which includes determining the learning rate, the number of network layers, the number of neurons, and the threshold function. Preliminary steps for the network include preprocessing and feature extraction of the input signal, and then testing on multiple modes to match suitable ones. Thereafter, the network is trained according to the set rules until it produces output results that comply with these rules. The basic process of BPNN and small DC motor characteristic signal identification is shown in Fig. 6.

Based on the above operations, the final data prediction algorithm based on BPNN can include three steps: building BPNN, training BPNN and predicting data. The specific process and the built neural network training results are shown in Fig. 7.

4. TESTING AND APPLICATION OF MECHANICAL NOISE CONTROL METHODS

In order to ensure In order to verify the superior performance and applicability of the proposed method (EMI-BP) in the experiment, the fuel cell bidirectional DC motor control method based on neural network estimation adaptive sliding mode technology (Adaptive sliding mode technology-neural network estimation, ASMT-ANN) was selected, Intelligent control method of electromagnetic pulse characteristics of digital controller based on deep semantic segmentation and time-frequency analysis (CNN-DeepLabV3+), Active damping stability improvement method of DC microgrid based on neural network and model predictive control (ANN-MPC) and research Methods for performance comparison [28-30]. Experimental analysis is conducted on the four algorithms and the experiments are conducted in the same simulation environment.

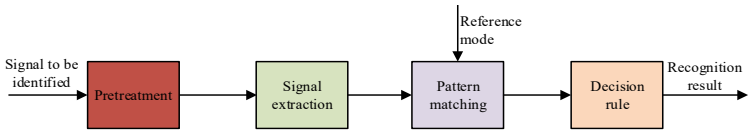

Fig. 6. BPNN process and signal recognition process

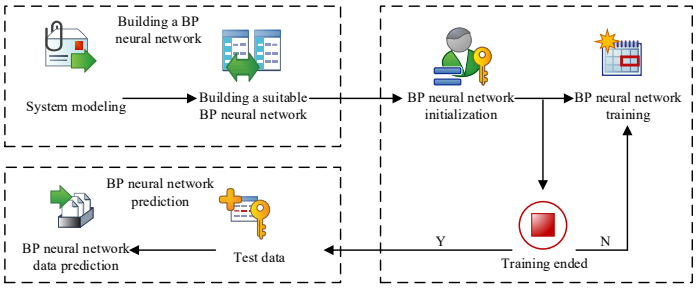

Fig. 7. Architecture of BPNN

The schematic diagram of the simulated motor structure is shown in Fig. 8.

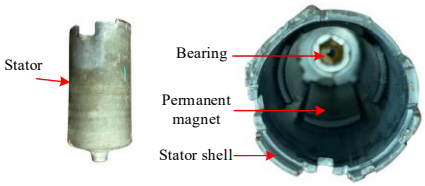

(a) Schematic diagram of stator structure

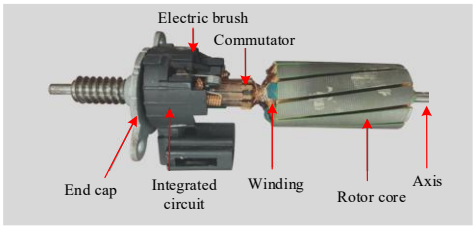

(b) Schematic diagram of the motor structure used in the experiment

Fig. 8. Schematic diagram of the motor structure used in the experiment

The relevant parameters of the simulation environment are shown in Table 1.

Table 1. Setting of relevant parameters

Experimental equipment	Parameters
CPU	Intel Core i9-10900K
GPU	NVIDIA RTX 3080
Memory	32GB DDR4
Graphics memory	10GBGDDR6X
Development environment	Windows 10, Python 3.8
Programming tools	PyTorch 1.7
Analysis software	ANSYS

The experiment selected the noise data set Mendeley Data as the task data set, selected 6000 valid data from this data set, and randomly grouped the data set. 30% of the data is used as the training set, and the other 70% of the data is used as the test set. First, the convergence speed of the four algorithms running on the two data sets is compared. The specific results are shown in Fig. 9.

Fig. 9(a) shows the changes in fitness values of different algorithms running on the training set. As the amount of data increases, the fitness values of the four algorithms begin to increase to varying degrees. When the amount of data increases to 560, the fitness value of the EMI-BP method has the maximum value, with a value as high as 98.98%; at this time, the fitness values of the three algorithms CNN-DeepLabV3+, ANN-MPC and ASMT-ANN do not. Reach a stable value. Fig. 9 (b) shows the change of fitness value on the test set. The fitness values of the four algorithms are also constantly changing. When the amount of data reaches 1120 and 1540 respectively, the fitness of EMI-BP and CNN-DeepLabV3+ methods becomes stable, with values of 97.86% and 92.12% respectively; while the fitness of other methods is still fluctuating. The above results prove that with the same amount of data, the EMI-BP method can reach the convergence state relatively quickly, and at the same time, the operation efficiency is faster. The changes in the accuracy of noise control by the four algorithms are shown in Fig. 10.

Fig. 10(a) shows the accuracy control changes of the four algorithms running on the training set. It can be found that as time increases, the accuracy of all models shows a downward trend. When the running time increases to 0.894 s, the EMI-BP method's control accuracy of mechanical noise reaches 91,68%.

At this time, the control accuracy rates of the other three methods are all on a downward trend. The accuracy rates of CNN-DeepLabV3+, ANN-MPC and ASMT-ANN are 90.34%, 89.61% and 88.54% respectively. Fig. 10(b) shows the accuracy control changes running on the test set. When the EMI-BP method starts to decrease, the accuracy values of the remaining three methods also start to decrease. When the running time is 0.921 s, the accuracy of the EMI-BP method begins to have a maximum value of 93.79%; at this time, the accuracy of other methods is significantly smaller than the research method.

From the comparison, it can be seen that there are significant differences in the accuracy values of the EMI-BP method and the other three comparison methods, which shows that the research method can effectively control the generation of mechanical noise of small DC motors and has a high accuracy.

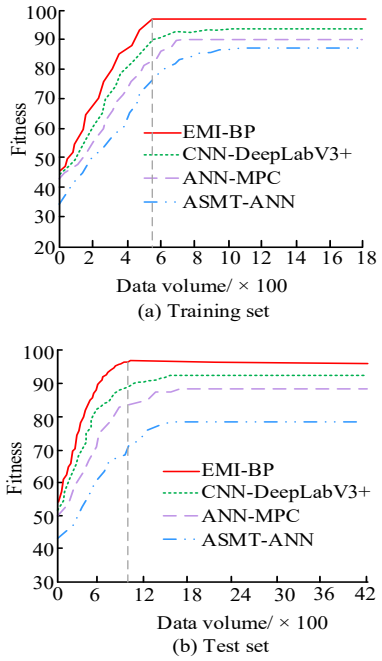

Fig. 9. Changes in convergence speed of different algorithms

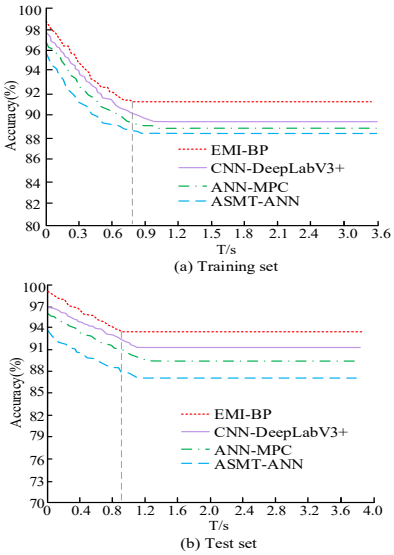

Fig. 10. Changes in accuracy of noise control using different algorithms

Based on the above analysis, in order to verify the practical application effect of the method constructed in the experiment, four different algorithms were applied to a small DC electrode. Under the condition of ensuring that all experimental factors are the same, ANSYSWORKBENCH is first used to conduct simulation experiments to obtain the natural frequency of the stator; at the same time, the thickness of the stator shell is set to 2.0 mm, 2.2 mm, 2.4 mm, 2.6 mm, 2.8 mm and 3.0 mm, and the stator is analyzed. Effect of shell thickness on natural frequencies. See Fig. 11 for specific results.

Fig. 11(a) shows the stator piezoelectric simulation diagram. It can be found that the displacements produced by the stator at 4400, 6050, 9530, 10250, 11560, 14480 and 15540 Hz are more prominent, indicating that these seven frequency points are the natural frequencies of the stator. Fig. 11(b) shows the effect of different stator shell thicknesses on natural frequency. As the natural frequency of the six orders increases, it can be seen that there is a positive correlation between the natural frequency of the stator and the thickness of the stator. The natural frequency of the stator is significantly affected by the thickness of the stator shell.

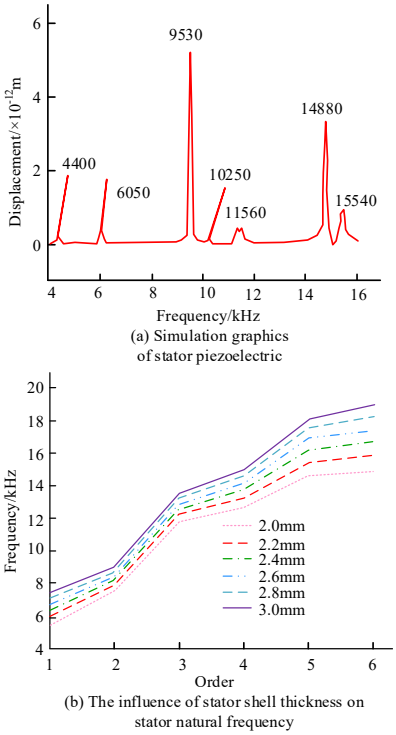

Fig. 11. Simulation graphics of stator piezoelectric and changes in stator natural frequency

Then, keeping the experimental conditions and factors unchanged, aluminum alloy, cast iron, steel and copper were selected as stator shell materials, and the changes in natural frequency were analyzed. The Poisson's ratios of aluminum alloy, cast iron, steel and copper are 0.33, 0.25, 0.24-0.28 and 0.34 respectively. The elastic moduli of aluminum alloy, cast iron, steel and copper are 70 GPa, 120 GPa, 200 GPa and 110-128 GPa respectively. The specific results are shown in Fig. 12.

Fig. 12(a) shows the influence of different stator materials on the natural frequency of the stator. It can be found that as the order increases, the order of natural frequencies of the four materials is steel > aluminum alloy > cast iron > copper. However, the Poisson's ratio and elastic modulus of steel are not the largest values among the four materials. In order to verify the reason for

this phenomenon, the experiment kept other factors unchanged, assuming that the stator shell construction material is steel, and only changed the stator shell material density, to analyze the effect of material density on natural frequency. The specific

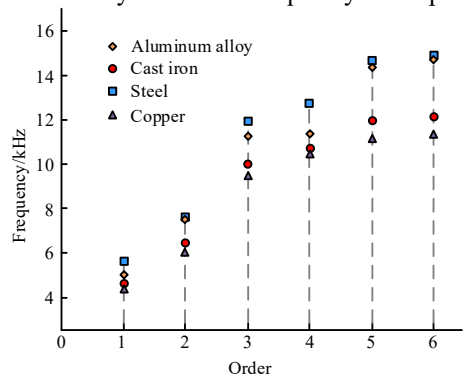

(a) The influence of stator material on stator natural frequency

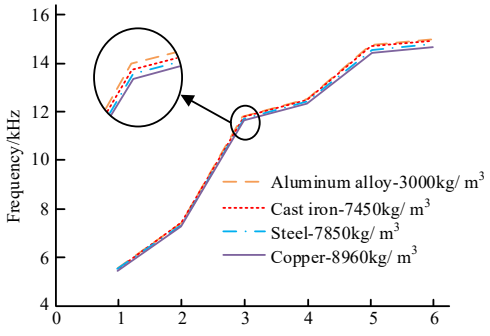

(b) The influence of material density on the natural frequency of stator

Fig. 12. Effect of stator material and material density on stator natural frequency

results are shown in Fig. 12(b). As the material density increases, the natural frequency of the stator begins to decrease; but the natural frequency of the stator decreases to a smaller extent, which also proves that the material density of the stator has a small impact on the natural frequency of the stator. It can be seen that when the material is steel, the value of the stator's natural frequency changes greatly. Then only the elastic modulus of the stator is changed, and the influence of the elastic modulus on the natural frequency of the stator is analyzed respectively; the Poisson's ratio of the steel is changed, and the influence of different Poisson's ratios on the modal frequency of the steel is analyzed. See Fig. 13 for details.

Fig. 13(a) shows the effect of changes in elastic modulus on the natural frequency of the stator. It is observed that the elastic modulus growth causes the natural frequency to rise significantly and reaches a maximum value when the elastic modulus is 200 GPa. This shows that when steel is used as a material, its elastic modulus is one of the important factors affecting the natural frequency of the stator. Fig. 13(b) analyzes the effect of Poisson's ratio on the stator modal frequency. In the range of Poisson's ratio from 0.2 to 0.35, its change has little effect on the stator modal frequency, indicating that the Poisson's ratio of the steel material has a slight impact on the natural frequency. Generally speaking, when the stator shell material is steel, its maximum natural frequency is mainly affected by changes in elastic modulus and material density, among which the elastic modulus plays a more significant role.

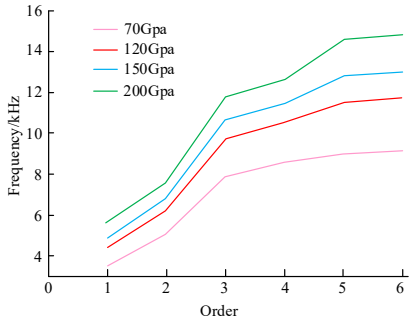

(a) The influence of elastic modulus on the natural frequency of stator

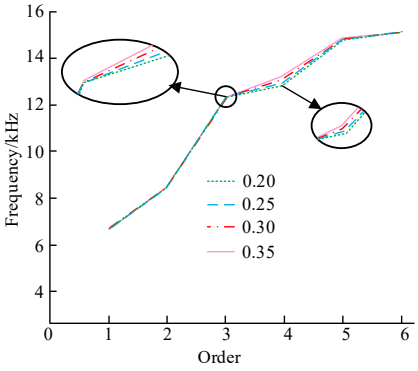

(b) The influence of Poisson's ratio on stator modal frequency

Fig. 13. Poisson's ratio and elastic modulus's effects on stator natural frequency

5. CONCLUSION

The study analyzed the problem that small DC electrodes are prone to mechanical noise during operation, and proposed a mechanical noise control method that combines electromagnetic interference and BPNN. Through a series of experiments and theoretical analysis, the feasibility and effectiveness of the improved BP technology in optimizing electrode noise control of small DC motors were successfully verified, thereby significantly reducing mechanical noise. The data shows that when running on the training set and test set, the fitness value of the EMI-BP method always has the maximum value, with values as high as 98.98% and 97.86% respectively. In addition, when running on the test set, the EMI-BP method started to have a maximum accuracy of 93.79% when the system ran for 0.921s. The constructed method was applied to the operation of a small DC motor electrode and found that assuming the material is steel, the elastic modulus has the most obvious

impact on the maximum natural frequency of the stator, and the impact of the elastic modulus on the natural frequency is much greater than the material density. The above results show that the research method not only provides a new technical approach to the mechanical noise control of small DC motor electrodes, but also provides a new theoretical and practical reference for research in the field of electromagnetic interference.

However, the research only verified the effectiveness of the proposed method in the laboratory environment. In practical industrial applications, the complexity of equipment operating conditions such as temperature and humidity changes may affect the stability and accuracy of the method. In addition, the training process of BPNN requires high computing resources, which limits its application in resource-constrained environments. The future work will expand the experiment to the actual industrial environment, optimize the neural network architecture to improve the calculation efficiency, and deeply analyze the influence of dynamic electromagnetic field on mechanical noise, so as to further improve the practicability and reliability of the method.

Source of funding: *This research received no external funding.*

Author contributions: *research concept and design, H.C., X.Z.; Collection and/or assembly of data, H.C., X.Z.; Data analysis and interpretation, H.C., X.Z.;Writing the article, H.C., X.Z.; Critical revision of the article, H.C., X.Z.; Final approval of the article, H.C., X.Z.*

Declaration of competing interest: *The author declares no conflict of interest.*

Data Availability Statement: *The data used to support the findings of this study are all in the manuscript.*

REFERENCES

1. Ranjbar E, Yaghubi M, Abolfazl Suratgar A. Robust adaptive sliding mode control of a MEMS tunable capacitor based on dead-zone method. Automatika: Časopis Za Automatiku, Mjerenje, Elektroniku, Računarstvo I Komunikacije, 2020;61(4):587-601. https://doi.org/10.1080/00051144.2020.1806011.
2. Simon K, Vicent M, Addah K, Bamutura D, Atwiine B, Nanjebe D, Mukama AO. Comparison of deep learning techniques in detection of sickle cell disease. Artificial Intelligence and Applications. 2023;1(4): 252-259. https://doi.org/10.47852/bonviewAIA3202853.
3. Zhai L, Yang S, Hu G, Lv M. Optimal design method of high voltage dc power supply EMI filter considering source impedance of motor controller for electric vehicle. IEEE Transactions on Vehicular Technology. 2022;72(1):367-381. https://doi.org/10.1109/TVT.2021.3080924.
4. Preethi P, Mamatha HR. Region-Based convolutional neural network for segmenting text in Epigraphical images. Artificial Intelligence and Applications. 2023;1(2):119-127. https://doi.org/10.47852/bonviewAIA2202293.
5. Nelis JLD, Bose U, Broadbent JA, Hughes J, Sikes A, Anderson A, Colgrave ML. Biomarkers and biosensors for the diagnosis of noncompliant pH, dark cutting beef predisposition, and welfare in cattle. Comprehensive Reviews in Food Science and Food Safety. 2022;21(3):2391-2432. https://doi.org/10.1111/1541-4337.12935.
6. Xu C, Wang J, Chen D, Chen J, Liu B, Qi W, Zheng X. The electrochemical seismometer based on fine-tune sensing electrodes for undersea exploration. IEEE Sensors Journal. 2020;20(15):8194-8202. https://doi.org/10.1109/JSEN.2020.2985702.
7. Abd Aziz MA, Saidon MS, Romli MIF, Othman SM, Mustafa WA, Manan MR, Aihsan MZA. Review on BLDC motor application in electric vehicle (EV) using battery, supercapacitor and hybrid energy storage system: efficiency and future prospects. Journal of Advanced Research in Applied Sciences and Engineering Technology. 2023;30(2):41-59. https://doi.org/10.37934/araset.30.2.4159.
8. Abdullah Y, Shaffer J, Hu B, Hall B, & Arfaei B. Hurst-exponent-based detection of high-impedance DC arc events for 48-V systems in vehicles. IEEE Transactions on Power Electronics. 2020;36(4): 3803-3813. https://doi.org/10.1109/TPEL.2020.3020587.
9. Jiang Y, Liu L, Chen L, Zhang Y, He Z, Zhang W, Qin Y. Flexible and stretchable dry active electrodes with PDMS and silver flakes for bio-potentials sensing systems. IEEE Sensors Journal. 2021;21(10):12255-12268. https://doi.org/10.1109/JSEN.2021.3061949.
10. Krasecki VK, Sharma A, Cavell AC, Forman C, Guo SY, Jensen ET, Goldsmith RH. The role of experimental noise in a hybrid classical-molecular computer to solve combinatorial optimization problems. ACS Central Science. 2023;9(7):1453-1465. https://doi.org/10.1021/acscentsci.3c00515.
11. Xu H, Zhang W, Deng J, Rabault J. Active flow control with rotating cylinders by an artificial neural network trained by deep reinforcement learning. Journal of Hydrodynamics. 2020;32(2): 254-258. https://doi.org/10.1007/s42241-020-0027-z.
12. Cao J, Wei X, Su Y, Shi H, Zhou D. Experimental analysis of electromagnetic pulse effects on engine fuel electronic control system. International Journal of Applied Electromagnetics and Mechanics. 2020; 65(6):1-13. https://doi.org/10.3233/JAE-190161.
13. Ge MY, Wang GW, Jia Y. Influence of the Gaussian colored noise and electromagnetic radiation on the propagation of subthreshold signals in feedforward neural networks. Science China Technological Sciences, 2021, 64(4): 847-857. https://doi.org/10.1007/s11431-020-1696-8.
14. Wang J, Liu Y, Jin Y, Zhang Y. Control of hydraulic power system by mixed neural network PID in unmanned walking platform. Journal of Beijing Institute of Technology. 2020;29(3):273-282.
15. Wang Q, Wang X. Parameters optimization of the heating furnace control systems based on BP neural network improved by genetic algorithm. IEEE

Internet of Things Journal. 2020;2(2):75-80. https://doi.org/10.32604/jiot.2020.010226.
16. Xue B, Li Y, Cheng Z, Yang S, Xie L, Qin S. Directional electromagnetic interference shielding based on step-wise asymmetric conductive networks. Nano-Micro Letters. 2022;14(1):262-277. https://doi.org/10.1007/s40820-021-00743-y.
17. Charles D. The Lead-Lag Relationship between international food prices, freight rates, and Trinidad and Tobago's food inflation: a support vector regression analysis. Green and Low-Carbon Economy. 2023;1(2):94-103. https://doi.org/10.47852/BONVIEWGLCE3202797.
18. Vafamand N, Arefi MM. Robust neural network-based backstepping landing control of quadrotor on moving platform with stochastic noise. International Journal of Robust and Nonlinear Control. 2022;32(4):2007-2026. https://doi.org/10.1002/rnc.5933.
19. Kanwisher N, Khosla M, Dobs K. Using artificial neural networks to ask 'why'questions of minds and brains. Trends in Neurosciences. 2023;46(3):240-254. https://doi.org/10.1016/j.tins.2022.12.008.
20. Goel A, Goel AK, Kumar A. The role of artificial neural network and machine learning in utilizing spatial information. Spatial Information Research. 2023;31(3):275-285. https://doi.org/10.1007/s41324-022-00494-x.
21. Kurani A, Doshi P, Vakharia A, Shah M. A comprehensive comparative study of artificial neural network (ANN) and support vector machines (SVM) on stock forecasting. Annals of Data Science. 2023; 10(1):183-208. https://doi.org/10.1007/s40745-021-00344-x.
22. Khan J, Lee E, Kim K. A higher prediction accuracy–based alpha–beta filter algorithm using the feedforward artificial neural network. CAAI Transactions on Intelligence Technology. 2023;8(4): 1124-1139. https://doi.org/10.1049/cit2.12148.
23. Shen H. Assessment of financial risk pre-alarm mechanism based on financial ecosystem using BPNN and genetic algorithm. Soft Computing. 2023;27(24): 19265-19279. https://doi.org/10.1007/s00500-023-09317-z.
24. Su K, Zhang J, Zhang J, Yan T, Mei G. Optimisation of current collection quality of high-speed pantograph-catenary system using the combination of artificial neural network and genetic algorithm. Vehicle System Dynamics. 2023;61(1):260-285. https://doi.org/10.1080/00423114.2022.2045029.
25. Tanhaeean M, Ghaderi S F, Sheikhalishahi M. Optimization of backpropagation neural network models for reliability forecasting using the boxing match algorithm: electro-mechanical case. Journal of Computational Design and Engineering. 2023;10(2): 918-933. https://doi.org/10.1093/jcde/qwad032.
26. Shen LB, Tian LP. A static load position identification method for optical fiber-composite structures based on particle swarm optimization-back Propagation neural network algorithm. Measurement and Control. 2023;56(3-4):820-831. https://doi.org/10.1177/0020294022110167.
27. Chi X, Quan S, Chen J, Wang YX, He H. Proton exchange membrane fuel cell-powered bidirectional DC motor control based on adaptive sliding-mode technique with neural network estimation. International Journal of Hydrogen Energy. 2020;45(39):20282-20292. https://doi.org/10.1016/j.ijhydene.2019.12.224.
28. Wei M, Chen K, Li S, Cao J, Ali A. An intelligent method based on time–frequency analysis and deep learning semantic segmentation for investigating the electromagnetic pulse features of engine digital controllers. IEEE Transactions on Electromagnetic Compatibility. 2022;65(1):257-270. https://doi.org/10.1109/TEMC.2022.3218717.
29. Zhao D, Shen K, Chen L, Wang Z, Liu W, Yang T, Wheeler P. Improved active damping stabilization of DAB converter interfaced aircraft DC microgrids using neural network-based model predictive control. IEEE Transactions on Transportation Electrification. 2021;8(2):1541-1552. https://doi.org/10.1109/TTE.2021.3094757.

Hui CAO (1981) Born in Xincai County, Henan province. Chinese Communist Party members, received his Master of Science from Nanjing University of Science and Technology in 2007 , Condensed Matter Physics Major. He is currently an associate professor in Henan Polytechnic Institute. His research interests include applied physics, mechanics and mechanical-electrical integration, Published more than 10 papers at home and abroad.
e-mail: caohui1003@126.com

Xiaoyan ZHANG (1988) Born in Yushu City, Jilin Province. Chinese Communist Party members, received her Bachelor of Engineering degree from Shandong Institute of Light Industry in 2011.Process equipment and control engineering. She taught at the 13th Division vocational and Technical School of Xinjiang Production and Construction Corps. The main research direction is mechanical and electrical.
e-mail: zhangxiaoyan4332@126.com